Analysis of spin-dependent tunnelling of electrons in solid state structures using the transfer-Hamiltonian method

1997 J. Phys.: Condens. Matter 9 10651

(http://iopscience.iop.org/0953-8984/9/48/009)

J. Phys.: Condens. Matter **9** (1997) 10651–10660. Printed in the UK PII: S0953-8984(97)83487-X

Analysis of spin-dependent tunnelling of electrons in solid state structures using the transfer-Hamiltonian method

H J Reittu

Wihuri Physical Laboratory, University of Turku, 20014 Turku, Finland

Received 15 April 1997, in final form 4 September 1997

Abstract. The transfer-Hamiltonian (t-H) method is applied to study spin-dependent low-rate transfer of electrons between magnetically ordered metallic electrodes separated by a potential barrier. A weak coupling of the electrodes through the potential barrier is described with help of a t-H treated as a perturbation. Spin-dependent tunnelling probability amplitudes are expressed by a 2×2 matrix with elements evaluated through an overlap between the spinor components of the electron wavefunctions from both sides of the potential barrier, resulting in spin-dependent tunnelling current and tunnelling conductance. In particular, the magnetic valve effect in tunnelling between two ferromagnets and elements of the theory of a spin-polarized scanning tunnelling microscope with a ferromagnetic tip are analysed. The t-H method is useful also in applications to tunnelling in magnetic nanostructures and multilayers.

1. Introduction

Spin-polarized tunnelling phenomena have been studied quite extensively during recent years. Early experiments in this field [1] were made using junctions of thin ferromagnetic and superconducting films separated by an oxide layer. Julliere [2] was the first to show that the tunnelling conductance between two ferromagnetic films depends on relative orientation of their magnetizations. Spin-dependent transport phenomena are also responsible for the 'giant magnetoresistance' in magnetic multilayers [3]. The magnetoresistance appearing in tunnelling junctions is called tunnelling magnetoresistance. In magnetic nanostructures its magnitude can be of the order of the giant magnetoresistance [4, 5].

An interesting field of spin-polarized tunnelling phenomena is spin-polarized scanning probe microscopy (SPSPM). Several authors have proposed such devices utilizing various types of tip material. These include ferro- or antiferromagnetic tips [6–8] or optically pumped nonmagnetic semiconductors [9–18]. In SPSPM images it should be possible to detect spin asymmetry of the tunnelling current or that of the force acting between the tip and the sample [17]. Then it is possible to probe magnetic properties of the sample surface with a very high spatial resolution.

The transfer-Hamiltonian (t-H) method was developed by Oppenheimer [19] in 1928 for treating tunnelling problems in atomic physics. Later Bardeen extended it to tunnelling in solid state structures [20]. In the t-H method a potential barrier is regarded separating the system to two parts coupled weakly by a transfer Hamiltonian that can be treated as a perturbation in time-dependent perturbation theory. This approach has been very useful in applications like theory of scanning tunnelling microscopy (STM) [21] and theory of tunnelling between superconductors [20].

0953-8984/97/4810651+10$19.50

As we shall show the t-H method can be applied to spin-polarized tunnelling when the corresponding Hamiltonian contains operators acting on the spin degree of freedom. The approximate solution of the tunnelling problem is written in terms of wavefunctions of uncoupled systems. Thus even if they are not known explicitly, as in the case of an arbitrary potential barrier, it is still possible to reveal the physical meaning of the spin-dependent tunnelling characteristics writing them in terms of those wavefunctions. This is interesting since such magnitudes carry information about magnetic properties of the electrodes. For instance, in the theory of spin-polarized STM such analysis helps us to understand the physical contents of the images obtained with this device. The t-H method allows extensions of the well known approach based on analysis of spin-polarized tunnelling effects using an exactly solvable rectangular potential barrier problem [22–25] towards an arbitrary potential barrier when the two electrodes are well separated from each other (the 'weak-coupling' limit). In a particular case of a nonmagnetic optically pumped tip and a ferromagnetic sample the tunnelling current and the exchange force have been calculated using the t-H method [14, 16–18]. In the following we generalize the t-H description of spin-polarized electron tunnelling to electrodes having any type of spin order. An effective one-electron picture is used in the calculations.

2. Tunnelling matrix elements for spin-polarized tunnelling

Let us consider two magnetically ordered metals that are labelled as l (left) and r (right) in figure 1. They are separated by a relatively wide vacuum gap in the middle of which a separation surface S is situated. The volume to left (right) of S is denoted as V_l (V_r). In the following we adopt an effective one-electron picture similar to that used e.g. by Slonczewski in his theory of spin-polarized tunnelling between two ferromagnets [22].

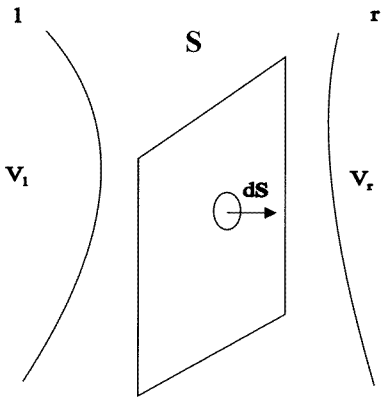

Figure 1. Location of the separation surface $\boldsymbol{S}$ between the metallic electrodes at left (l) and at right (r). The space to left or right from $\boldsymbol{S}$ is denoted by V_l and V_r respectively. d$\boldsymbol{S}$ is a vector element normal to the surface $\boldsymbol{S}$ pointing out from the volume V_l.

At first we consider an infinitely wide vacuum gap through which the electron tunnelling is impossible (see the discussion after (4)). The stationary electronic states are eigenstates of the Hamiltonian

$$H_i = T + U_i \tag{1}$$

with $i = l, r$, $T = (-\hbar^2/2m_e)\Delta$ and

$$(T + U_i)\Phi_i = E_i\Phi_i. \tag{2}$$

Here U_i is a 2×2 Hermitian matrix that acts on the spin degree of freedom (Φ_i is a two-component vector) of an electron. For such matrices there exist two independent eigenvectors denoted as $\Phi_{i1}(\boldsymbol{x})$ and $\Phi_{i2}(\boldsymbol{x})$. Their components can be expressed as

$$\Phi_{is}(\boldsymbol{x}) = \begin{pmatrix} \psi_{is,\uparrow}(\boldsymbol{x}) \\ \psi_{is,\downarrow}(\boldsymbol{x}) \end{pmatrix} = \psi_{is,\uparrow}(\boldsymbol{x}) \begin{pmatrix} 1 \\ 0 \end{pmatrix} + \psi_{is,\downarrow}(\boldsymbol{x}) \begin{pmatrix} 0 \\ 1 \end{pmatrix} \tag{3}$$

where $(1, 0)^T$ and $(0, 1)^T$ are transposed eigenvectors of the σ_z Pauli matrix and $\psi_{is,\sigma}(\boldsymbol{x})$ are functions describing the spatial dependence of the spinor components.

Now we assume a finite vacuum gap allowing low-rate tunnelling between the electrodes. We take the values of U_l and U_r in the vacuum to be zero (see also [21]). Then the total Hamiltonian can be written as (see figure 2)

$$H = T + U_l + U_r. \tag{4}$$

We assume that the wavefunctions $\Phi_{is}(\boldsymbol{x})$ in (2) and (3) have very small amplitude at distances from the surface of the order of d or greater (see figure 2). As a consequence these wavefunctions have only a small overlap with each other. The smallness of the overlap allows the construction of a perturbation theory for spin-polarized electron tunnelling as in the t-H approach to the problem of unpolarized tunnelling [21]. It should be noted that the representation of the Hamiltonian (4) is not unique since the choice of 'unperturbed' Hamiltonian is a matter of convenience. The unperturbed wavefunctions do not necessarily represent those of independent subsystems (see the discussion of this question in [21]). The optimal choice of the Hamiltonian that minimizes errors of the first-order perturbation theory is described in Chen's book [21] (see also figure 2). In this form the t-H method contains effectively [21] a part of the changes of the tunnelling characteristics caused by the interaction between the electrodes and thus provides a better approximation than the traditional t-H [20]. In the following we assume that Φ_{is} and the potentials U_i correspond to the optimal choice of the Hamiltonian defined in [21].

Considering transitions from left to the right the operator U_r is treated as a perturbation causing the transitions. Such transitions are most effective when $E_l \approx E_r = E$ [26]. Then we can find the wavefunction with help of the *ansatz*

$$\psi(\boldsymbol{x}, t) \approx \sum_{is} a_{is}(t)\Phi_{is}(\boldsymbol{x})\,\mathrm{e}^{-\frac{\mathrm{i}Et}{\hbar}}. \tag{5}$$

By substituting (5) into the time-dependent Schrödinger equation we obtain

$$\mathrm{i}\hbar \sum_{is} \dot{a}_{is}(t)\Phi_{is}(\boldsymbol{x}) = \sum_{s} (a_{ls}(t)U_r\Phi_{ls}(\boldsymbol{x}) + a_{rs}(t)U_l\Phi_{rs}(\boldsymbol{x})). \tag{6}$$

The scalar product of both sides of (6) with $\Phi_{ls'}$ yields

$$\mathrm{i}\hbar\dot{a}_{ls'}||\Phi_{ls'}||^2 = \sum_{s} \left(a_{ls} \int_{V_r} \Phi^+_{ls'} U_r \Phi_{ls}\,\mathrm{d}V + a_{rs} \int_{V_l} \Phi^+_{ls'} U_l \Phi_{rs}\,\mathrm{d}V \right) \tag{7}$$

where superscript $+$ denotes the Hermitian conjugate matrix. Since $\Phi_{ls'}$ decays exponentially inside the volume V_r the first integral in (7) can be neglected. Taking also into account that U_l is a Hermitian matrix and the equation $(U_l\Phi_{ls'})^* = (E - T)\Phi^*_{ls'}$ (7) can be written as

$$\mathrm{i}\hbar\dot{a}_{ls'} \approx \sum_{s} a_{rs} \int_{V_l} (\Phi^+_{rs} U_l \Phi_{ls'})^*\,\mathrm{d}V = \sum_{s} a_{rs} \int_{V_l} (\Phi^+_{rs}(E - T)\Phi_{ls'})^*\,\mathrm{d}V. \tag{8}$$

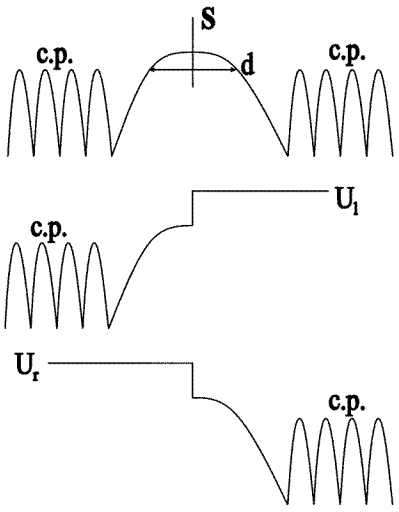

Figure 2. Schematic view of the potential profile (top graph) of the two electrodes separated by a potential barrier of width d. The separation surface $\boldsymbol{S}$ is located roughly in the middle of the barrier. Within each electrode there is a periodic crystal potential (c.p.). The two lower graphs show the potentials U_l and U_r used for calculation of the tunnelling probability amplitudes of the electrons with the t-H approach. The jumps of U_l and U_r at the surface $\boldsymbol{S}$ correspond to the optimal choice of unperturbed Hamiltonians [21] that minimize errors in the first-order perturbation theory. According to this the potentials have beyond the separation surface a constant value that is equal to the vacuum level taken here as the zero level of potential energy.

Applying the Green theorem to the term containing the operator T and the equation

$$\int_{V_l} \Phi_{ls}^{+} T \Phi_{rs'} \, \mathrm{d}V = E \int_{V_l} \Phi_{ls}^{+} \Phi_{rs'} \, \mathrm{d}V \tag{9}$$

(8) can be transformed into

$$\mathrm{i}\hbar \dot{a}_{ls'}(t) \approx \sum_{s} M_{ls',rs} a_{rs}(t) \tag{10}$$

where

$$M_{ls',rs} = \frac{\hbar^2}{2m_e} \int \mathrm{d}\boldsymbol{S} \cdot [(\Phi_{rs}^{+} \nabla \Phi_{ls'})^* - \Phi_{ls'}^{+} \nabla \Phi_{rs}] \tag{11}$$

are tunnelling matrix elements. Here $\mathrm{d}\boldsymbol{S}$ is an element of the separation surface between the volumes V_l and V_r (see figure 1).

With an analogous treatment it can be verified that

$$\mathrm{i}\hbar \dot{a}_{rs'}(t) \approx \sum_{s} M_{rs',ls} a_{ls}(t) \tag{12}$$

where

$$M_{rs',ls} = -\frac{\hbar^2}{2m_e} \int \mathrm{d}\boldsymbol{S} \cdot [(\Phi_{ls}^{+} \nabla \Phi_{rs'})^* - \Phi_{rs'}^{+} \nabla \Phi_{ls}] \tag{13}$$

and $\mathrm{d}\boldsymbol{S}$ has the same direction as in (11).

The elements $M_{rs',ls}$ form a 4×4 matrix (M). By denoting $\boldsymbol{a}(t) = (a_{l1}(t), a_{l2}(t), a_{r1}(t), a_{r2}(t))^T$ (10) and (12) can be written as

$$\mathrm{i}\hbar \dot{\boldsymbol{a}}(t) \approx M\boldsymbol{a}(t). \tag{14}$$

According to (11) and (13) $M_{rs',ls} = M^*_{ls,rs'}$ and we can define a matrix m with elements

$$m_{s',s} = M_{ls',rs}. \tag{15}$$

Then

$$M = \begin{pmatrix} \mathbf{0} & m \\ m^+ & \mathbf{0} \end{pmatrix} \tag{16}$$

where $\mathbf{0}$ is a 2×2 matrix with all components equal to zero.

3. Calculation of the tunnelling current and the conductance

Consider low-rate tunnelling from state $|\mathrm{ls}'\rangle$ to $|\mathrm{rs}\rangle$. Thus the initial conditions are

$$a_{ls'}(0) = 1 \qquad a_{rs}(0) = 0. \tag{17}$$

It is further assumed that a_{rs} is always kept near zero while $a_{ls'} \approx 1$. That is why (14) yields

$$\mathrm{i}\hbar\dot{a}_{rs}(t) \approx M_{rs,ls'}a_{ls'}(t). \tag{18}$$

Applying Fermi's golden rule [26] the tunnelling rate can be expressed as

$$\frac{\mathrm{d}|a_{rs}|^2}{\mathrm{d}t} \approx \frac{2\pi}{\hbar}|m_{ss'}|^2\delta(E_l - E_r). \tag{19}$$

The total current between the states $|\mathrm{ls}'\rangle$ and $|\mathrm{rs}\rangle$ is obtained summing over all relevant states. We assume a bias voltage V between the two parts. When statistical equilibrium is maintained in both electrodes the occupation number of each energy state is given by the Fermi distribution $f(E) = \{1 + \exp[(E - E_F)/k_BT]\}^{-1}$ with E_F being the Fermi energy and k_BT the temperature in energy units.

By introducing the density of state factors $N_{ls'}$ and N_{rs} the tunnelling current from state $|\mathrm{ls}'\rangle$ to state $|\mathrm{rs}\rangle$ is

$$I_{ls',rs} = \frac{2\pi e}{\hbar}\int \mathrm{d}E N_{ls'}(E - eV)N_{rs}(E)f(E - eV)[1 - f(E)]|m_{s,s'}|^2. \tag{20}$$

Analogously we find the reverse current between states $|\mathrm{ls}'\rangle$ and $|\mathrm{rs}\rangle$ as

$$I_{rs,ls'} = \frac{2\pi e}{\hbar}\int \mathrm{d}E\, N_{ls'}(E - eV)N_{rs}(E)f(E)[1 - f(E - eV)]|m_{s,s'}|^2. \tag{21}$$

The net current between these states is

$$I_{s,s'} = I_{ls',rs} - I_{rs,ls'} = \frac{2\pi e}{\hbar}\int \mathrm{d}E\, N_{ls'}(E - eV)N_{rs}(E)[f(E - eV) - f(E)]|m_{s,s'}|^2 \tag{22}$$

and the total current formed by summing over all tunnelling transitions is

$$I = \sum_{s,s'} I_{s,s'} = \frac{2\pi e}{\hbar}\int \mathrm{d}E\,[f(E - eV) - f(E)]\sum_{s,s'} N_{ls'}(E - eV)N_{rs}(E)|m_{s,s'}|^2. \tag{23}$$

For $k_BT \ll E_F$ we can replace the Fermi distribution $f(E)$ with a step function and write

$$I = \frac{2\pi e}{\hbar}\sum_{s,s'}\int_{E_F}^{E_F+eV} \mathrm{d}E\, N_{ls'}(E - eV)N_{rs}(E)|m_{s,s'}|^2. \tag{24}$$

At a low voltage, corresponding to $eV \ll E_F$, (24) can be expressed as

$$I \approx \frac{2\pi e^2 V}{\hbar}\sum_{s,s'} N_{ls'}(E_F)N_{rs}(E_F)|m_{s,s'}|^2. \tag{25}$$

This gives by definition the tunnelling conductance

$$G = \frac{I}{V} \approx G_0 \sum_{s,s'} N_{ls'}(E_F) N_{rs}(E_F) |m_{s,s'}|^2 \tag{26}$$

where

$$G_0 = \frac{(2\pi)^2}{R_K} \tag{27}$$

and $R_K = h/e^2 = 25\,812.8\ \Omega$ is the von Klitzing constant.

4. Magnetic valve effect, magnetoresistance between two ferromagnets and elements of the theory of spin-polarized STM

As an example of application of the t-H method we consider the problem of a magnetic valve between two ferromagnets separated by a narrow vacuum gap. This problem has already been solved by Slonczewski [22] using an exact solution for spin-polarized free electron plane waves tunnelling through a rectangular potential barrier between two ferromagnets. Our approach allows extensions of this solution since it is not bound to a particular model of the potential barrier in the sense described in the introduction. As a result it is possible to obtain a physical interpretation of the magnetic valve effect in a more general case.

In our model (see also [22]) the spin-dependent part of the Hamiltonian H_i (see (1) and (2)) is

$$U_i' = -\boldsymbol{h}_i \cdot \boldsymbol{\sigma} \tag{28}$$

where $\boldsymbol{\sigma} = (\sigma_x, \sigma_y, \sigma_z)$ is the Pauli spin operator. The direction of the field $\boldsymbol{h}_i$ defines the direction of the quantization axis of the ferromagnet i. U_i' inside the barrier vanishes. We take the z-axis along $\boldsymbol{h}_l$ and assume that $\boldsymbol{h}_r$ is tilted by an angle θ with respect to this direction. In this geometry

$$U_l' = h_l \sigma_z = -h_l \begin{pmatrix} 1 & 0 \\ 0 & -1 \end{pmatrix} \tag{29}$$

and

$$U_r' = -h_r \cos\theta\, \sigma_z - h_r \sin\theta\, \sigma_y = -h_r \begin{pmatrix} \cos\theta, & -\mathrm{i}\sin\theta \\ \mathrm{i}\sin\theta, & -\cos\theta \end{pmatrix}. \tag{30}$$

We find that the wavefunctions in (3) have the form

$$\Phi_{l1} = \chi_\uparrow(\boldsymbol{x}) \begin{pmatrix} 1 \\ 0 \end{pmatrix} \text{ and } \Phi_{l2} = \chi_\downarrow(\boldsymbol{x}) \begin{pmatrix} 0 \\ 1 \end{pmatrix} \tag{31}$$

where the wavefunctions $\chi_\sigma(\boldsymbol{x})$ depend on the particular form of the crystal potential. $\Phi_{l1}(\Phi_{l2})$ is simply the spin-up (spin-down) state that is an eigenfunction of σ_z with eigenvalue $+1$ (-1). The spinors Φ_{rs} have an analogous structure and are obtained by using the spinor transformation [28]

$$\Phi_{r1} = \xi_\uparrow(\boldsymbol{x}) \begin{pmatrix} \cos(\theta/2) \\ \mathrm{i}\sin(\theta/2) \end{pmatrix} \text{ and } \Phi_{r2} = \xi_\downarrow(\boldsymbol{x}) \begin{pmatrix} \sin(\theta/2) \\ -\mathrm{i}\cos(\theta/2) \end{pmatrix}. \tag{32}$$

By substituting (31) and (32) into (11), (13) and (15) we get in the one-dimensional case the following tunnelling matrix

$$m = \frac{\hbar^2 \kappa}{m_e} \begin{pmatrix} \xi_\uparrow^* \chi_\uparrow \cos(\theta/2) & \xi_\downarrow^* \chi_\uparrow \sin(\theta/2) \\ \mathrm{i}\xi_\uparrow^* \chi_\downarrow \sin(\theta/2) & -\mathrm{i}\xi_\downarrow^* \chi_\downarrow \cos(\theta/2) \end{pmatrix}. \tag{33}$$

Here the wavefunctions are taken in the middle of the vacuum gap where the separation plane $\boldsymbol{S}$ is located. κ is the decay constant of the wavefunctions ξ_σ and χ_σ in the vacuum region. Using these assumptions we can find from (26) the tunnelling conductance at low voltages:

$$G = G_0'[\rho_l(x_0, E_F)\rho_r(x_0, E_F) + m_l(x_0, E_F)m_r(x_0, E_F)\cos\theta] \tag{34}$$

where $G_0' = -(\hbar^2\kappa/m_e)G_0$. $\rho_i(x_0, E_F)$ and $m_i(x_0, E_F)$ are electronic local density of states (LDOS) and the electronic local spin density of the ith ferromagnetic electrode at point x_0 and at energy E_F, respectively. These functions can be simply expressed as

$$\rho_l(x_0, E_F) = N_{l1}|\chi_\uparrow(x_0)|^2 + N_{l2}|\chi_\downarrow(x_0)|^2 \tag{35}$$

and

$$m_l(x_0, E_F) = N_{l1}|\chi_\uparrow(x_0)|^2 - N_{l2}|\chi_\downarrow(x_0)|^2. \tag{36}$$

The spin-dependent part of the tunnelling conductance is proportional to the scalar product of the local spin densities $\boldsymbol{m}_i(x_0, E_F)$ taken as vectors pointing along $\boldsymbol{h}_i$. Such spin densities have been calculated numerically for several magnetic surfaces and overlayers [27] although only one surface was considered. As discussed above (after (4)) one electrode distorts the wavefunctions at the surface of the other electrode, thus affecting its spin-dependent character. However, when properly used the t-H method in conjunction with numerical simulations is capable of giving predictions about experimentally observable magnitudes.

The local degree of spin polarization is defined as $\boldsymbol{P}_i = \boldsymbol{m}_i/\rho_i$. Then the tunnelling conductance from (34) takes the form

$$G = G_0'\rho_l\rho_r(1 + P_lP_r\cos\theta) \tag{37}$$

and the tunnelling resistance is

$$R = G^{-1} = R_0(1 + P_lP_r\cos\theta)^{-1}. \tag{38}$$

Thus R is a periodic function of θ with an amplitude which depends on the mutual orientation of the magnetization of the ferromagnets on both sides of the junction. The maximum relative variation is

$$\Delta R/R = (R_A - R_P)/R_A = 2P_lP_r/(1 + P_lP_r) \tag{39}$$

where R_A and R_P are the junction resistances with antiparallel and parallel orientations of the magnetizations, respectively. Such a relation was given for the first time by Julliere who also made the first experiments to observe the effect [2]. However the t-H analysis above shows that in general the polarization appearing in the valve constant is not the bulk value but represents the local polarization under influence of the barrier. This can be an important point while evaluating the magnitude of the valve effect investigated recently (see [5] and references therein). For instance, tunnelling in a ferromagnet–insulator–ferromagnet (FM_1–I–FM_2) trilayer thin-film planar junction has been experimentally investigated [5]. The FM films had different coercive forces ($H_{C1} > H_{C2}$). In such a situation the tunnelling resistance depends on the magnitude of the applied magnetic field and is observed as a large magnetoresistance of the junction. When rotating the trilayer junction in a magnetic field between the limits $H_{C2} < H < H_{C1}$ the magnetization in FM_2 follows the direction of the magnetic field and it is possible to change gradually the angle θ between the magnetizations. Measurement of R was found to follow the periodic dependence on θ according to (38) although its actual shape could not be perfectly fitted with the cosine dependence. This deviation was addressed to nonidealities of the trilayer junction.

As an simplified example we analyse the magnetic valve in the case of a rectangular barrier [22]. The result of [22] is simply obtained by substituting in (33)–(38) the functions

$$\chi_\sigma(x) = \frac{2k_{l\sigma}}{k_{l\sigma} + \mathrm{i}\kappa}\,\mathrm{e}^{-\kappa(x+d)} \qquad \kappa = \sqrt{\frac{2m_e(-E)}{\hbar^2}} \qquad k_{l\sigma} = \sqrt{\frac{2m_e(U_0 + E \pm h_l)}{\hbar^2}} \tag{40}$$

and

$$\xi_\sigma(x) = \frac{2k_{r\sigma}}{k_{r\sigma} + \mathrm{i}\kappa}\,\mathrm{e}^{\kappa(x-d)} \qquad k_{r\sigma} = \sqrt{\frac{2m_e(U_0 + E \pm h_r)}{\hbar^2}} \tag{41}$$

where U_0 is a constant and the energy $E < 0$. (40) and (41) give the tails of free-electron type wavefunctions continued into the vacuum region. However, a rectangular surface potential is hardly a realistic choice since the surface potential is smooth in the atomic scale. On the other hand, calculations [29, 30] have been made showing that the effective one-electron surface potential is different for electrons with opposite spin projections. Qualitatively these potentials can be fitted with those in [29, 30] by replacing the step function $\Theta(x)$ in the rectangular potential with a function $g_{i\sigma}(x) = 1/(1 + \exp(-x/\alpha_{i\sigma}))$ where $\alpha_{i\sigma}$ ($i = l$ or r) is a parameter. At the limit $\alpha_{i\sigma} \to 0$ the function $g_{i\sigma}(x)$ approaches $\Theta(x)$. More precisely we write the spin dependent parts of the operators in (1) and (2) as

$$U_l'(x) = \begin{pmatrix} (U_0+h_l)/(1+\exp(-(x-d)/\alpha_{l\uparrow})-U_0-h_l) & 0 \\ 0 & (U_0-h_l)/(1+\exp(-(x-d)/\alpha_{l\downarrow})-U_0+h_l) \end{pmatrix} \tag{42}$$

and

$$U_r'(x) = \begin{pmatrix} (U_0+h_r)/(1+\exp((x+d)/\alpha_{r\uparrow})-U_0-h_r) & 0 \\ 0 & (U_0-h_r)/(1+\exp((x+d)/\alpha_{r\downarrow})-U_0+h_r) \end{pmatrix} \tag{43}$$

where U_0 is a constant. The wavefunctions corresponding to the operators $U_l'(x)$ and $U_r'(x)$ may be found in a way analogous to [14]. By substituting them into (33)–(37) we obtain

$$G = G_0'\rho_l\rho_r(1 + P_l P_r \cos\theta) \tag{44}$$

with

$$P_i = (A_{i\uparrow} - A_{i\downarrow})/(A_{i\uparrow} + A_{i\downarrow}) \tag{45}$$

and

$$A_{i\sigma} = (\kappa^2 + k_{i\sigma}^2)\,\sinh(2\pi k_{i\sigma}\alpha_{i\sigma})|\Gamma^2(\kappa\alpha_{i\sigma} - \mathrm{i}k_{i\sigma}\alpha_{i\sigma})|^2. \tag{46}$$

It can be seen that P_i is highly sensitive to the value of $\alpha_{i\sigma}$ when it changes in the range of a few ångström units [14]. Generally P_i approaches 1 [14] when $\alpha_{i\sigma}$ grows. This increases the magnetic valve effect in agreement with recent experimental results ($\Delta R/R$ close to 25%). For $\alpha_{i\sigma} \approx 0$ the value of P_i coincides with Slonczewski's result [22] $P_i = (k_{i\uparrow} - k_{i\downarrow})(\kappa^2 - k_{i\uparrow}k_{i\downarrow})/(k_{i\uparrow} + k_{i\downarrow})(\kappa^2 + k_{i\uparrow}k_{i\downarrow})$ according to which P_i can have low values or it can even be negative depending on the barrier height ($\propto \kappa^2$). These two examples clarify our method. However, as already pointed out it is in general necessary to use numerical simulations along with the t-H method to be able to find results for comparison with experiments.

Returning to the theory of SPSTM we should use a 3D approach instead of the 1D one as above. Here we adopt the method introduced by Chen [21]. In STM the tip (at the left) state may be considered as being always the same during an STM experiment while different sample (at the right) states are probed. Thus we should choose a particular tip state and consider an arbitrary sample state in (11) and (13). Only the vacuum tails of these

wavefunctions are required. Expanding the tip wavefunction into its spherical-harmonic components and taking into account only the spherically symmetric (s-state) part we get

$$\chi_\sigma(\boldsymbol{x}) \approx C_\sigma \exp(-\kappa|\boldsymbol{x}-\boldsymbol{x}_0|)/|\boldsymbol{x}-\boldsymbol{x}_0| \tag{47}$$

where $\boldsymbol{x}_0$ is the location of the nucleus of the apex atom. By applying the Chen derivative rule the tunnelling matrix can be expressed as

$$m \propto \begin{pmatrix} \xi^*_\uparrow(\boldsymbol{x}_0)C_\uparrow \cos(\theta/2) & \xi^*_\downarrow(\boldsymbol{x}_0)C_\uparrow \sin(\theta/2) \\ \mathrm{i}\xi^*_\uparrow(\boldsymbol{x}_0)C_\downarrow \sin(\theta/2) & -\mathrm{i}\xi^*_\downarrow(\boldsymbol{x}_0)C_\downarrow \cos(\theta/2) \end{pmatrix} \tag{48}$$

and the tunnelling conductance as

$$G \propto (1 + P_s(\boldsymbol{x}_0)P_t\ \cos(\theta)) \tag{49}$$

where $P_s(\boldsymbol{x}_0)$ is the local degree of spin polarization of the sample at the position of the tip apex. P_t is the asymptote of the degree of spin polarization of the tip at the vacuum gap and can be given in the form

$$P_t = \frac{N_{l1}|C_\uparrow|^2 - N_{l2}|C_\downarrow|^2}{N_{l1}|C_\uparrow|^2 + N_{l2}|C_\downarrow|^2}. \tag{50}$$

As a result spin-polarized STM images the local degree of spin polarization at the position of the tip apex, a result analogous to that by Hamann and Tersoff for normal STM [21]. Numerical calculations like those in [27] can be used to evaluate the corrugation amplitudes obtained with such devices using a ferromagnetic tip [6, 8].

5. Concluding remarks

The Bardeen transfer-Hamiltonian method is applied for description of electron spin-dependent tunnelling effects. Motivation for this comes from recent experimental investigations using spin-polarized scanning tunnelling microscopy and spin-dependent tunnelling current and exchange effects in magnetic nanostructures and multilayers.

Using the time-dependent perturbation theory the spin-dependent tunnelling probability amplitudes are expressed by a 2×2 matrix with elements evaluated through the overlap between the spinor components of the electron wavefunctions from both sides of the potential barrier. As a result spin-dependent tunnelling current and tunnelling conductance are found. In a particular case of tunnelling between two ferromagnets the magnetic valve effect is described. As another example of the spin-polarized t-H approach the physical meaning of surface images obtained on a ferromagnet with spin-polarized STM using a ferromagnetic tip is discussed.

Acknowledgments

The author is obliged to Professor Reino Laiho for valuable contributions and critical reading of the manuscript. Financial support to this work by the Academy of Finland is gratefully acknowledged.

References

[1] Meservey R, Tedrow P M and Fulde P 1970 *Phys. Rev. Lett.* **25** 1270
Tedrow P M and Meservey R 1971 *Phys. Rev. Lett.* **26** 192
[2] Julliere M 1975 *Phys. Lett.* **54A** 225

[3] Baibich M N, Broto J M, Fert A, Nguyen Van Day, Petroff F, Etienne P, Greuzet G, Friederich A and Chazelas J 1988 *Phys. Rev. Lett.* **61** 2472
[4] Maekawa S and Gefvert U 1982 *IEEE Trans. Magn.* **MAG-18** 707
[5] Moodera J S and Kinder L R 1996 *J. Appl. Phys.* **79** 4724
[6] Wiesendanger R, Güntherodt H-J, Güntherodt G, Gambino R J and Ruf R 1990 *Phys. Rev. Lett.* **65** 247
[7] Minakov A A and Shvets I V 1990 *Surf. Sci.* **236** L377
[8] Wiesendanger R, Shvets I V, Bürgler D, Tarrach G, Güntherodt H-J and Coey J M D 1992 *Europhys. Lett.* **19** 141
[9] Molotkov S N 1992 *Pis. Zh. Eksp. Teor. Fiz.* **55** 180
[10] Laiho R and Reittu H J 1993 *Surf. Sci.* **289** 363
[11] Sueoka K, Mukasa K and Hayakawa K 1993 *Japan. J. Appl. Phys.* **32** 2989
[12] Nunes G Jr and Amer N M 1993 *Appl. Phys. Lett.* **63** 1851
[13] Jansen R, van der Wielen M C M M, Prins M W J, Abraham D L and van Kempen H 1994 *J. Vac. Sci. Technol.* B **12** 2133
[14] Reittu H J 1994 *J. Phys.: Condens. Matter* **6** 1847
[15] Yamaguchi K, Okamoto K and Yugo S 1995 *J. Appl. Phys.* **77** 6061
[16] Prins M W J, van Kempen H, van Leuken H, de Groot R A, van Roy W and De Boeck J 1995 *J. Phys.: Condens. Matter* **7** 9447
[17] Reittu H J 1995 *Surf. Sci.* **334** 257
[18] Laiho R and Reittu H 1996 *Fiz. Tverd. Tela* **38** 918 (Engl. Transl. 1996 *Phys. Solid State* **38** 506)
[19] Duke C B 1969 *Tunnelling in Solids* (New York: Academic) pp 207–15
[20] Bardeen J 1961 *Phys. Rev. Lett.* **6** 57
[21] Chen C J 1993 *Introduction to Scanning Tunnelling Microscopy* (New York: Oxford University Press) pp 52–89
[22] Slonczewski J C 1989 *Phys. Rev.* B **39** 6995
[23] Hathaway K B and Cullen J R 1992 *J. Magn. Magn. Mater.* **104–107** 1840
[24] Erickson R P, Hathaway K B and Cullen J R 1993 *Phys. Rev.* B **47** 2626
[25] Erickson R P 1994 *J. Appl. Phys.* **75** 6163
[26] Davydov A S 1965 *Quantum Mechanics* (Oxford: Pergamon) pp 294–6
[27] Wu R and Freeman A J 1992 *Phys. Rev. Lett.* **69** 2867
[28] Pauli W 1973 *Wave Mechanics (Pauli Lectures on Physics 5)* (Cambridge, MA: MIT) pp 159–64
[29] Nagy D, Cutler P H and Feuchtwang T E 1979 *Phys. Rev.* B **19** 2964
[30] Nagy D 1979 *Surf. Sci.* **90** 102